IEICE TRANSACTIONS

on Electronics

DOI:10.1587/transele.2023ECP5046

Publicized:2024/05/20

A PUBLICATION OF THE ELECTRONICS SOCIETY

The Institute of Electronics, Information and Communication Engineers
Kikai-Shinko-Kaikan Bldg., 5-8, Shibakoen 3chome, Minato-ku, TOKYO, 105-0011 JAPAN

PAPER

Development of Microwave-Based Renal Denervation Catheter for Clinical Application

Shohei Matsuhara[†], ***Student Member***, **Kazuyuki Saito**[†], ***Member***, **Tomoyuki Tajima**[††], **Aditya Rakhmadi**[†], ***Member***, **Yoshiki Watanabe**[†††], **and Nobuyoshi Takeshita**[††††]

SUMMARY Renal Denervation (RDN) has been developed as a potential treatment for hypertension that is resistant to traditional antihypertensive medication. This technique involves the ablation of nerve fibers around the renal artery from inside the blood vessel, which is intended to suppress sympathetic nerve activity and result in an antihypertensive effect. Currently, clinical investigation is underway to evaluate the effectiveness of RDN in treating treatment-resistant hypertension. Although radio frequency (RF) ablation catheters are commonly used, their heating capacity is limited. Microwave catheters are being considered as another option for RDN. We aim to solve the technical challenges of applying microwave catheters to RDN. In this paper, we designed a catheter with a helix structure and a microwave (2.45 GHz) antenna. The antenna is a coaxial slot antenna, the dimensions of which were determined by optimizing the reflection coefficient through simulation. The measured catheter reflection coefficient is -23.6 dB using egg white and -32 dB in the renal artery. The prototype catheter was evaluated by *in vitro* experiments to validate the simulation. The procedure performed successfully with *in vivo* experiments involving the ablation of porcine renal arteries. The pathological evaluation confirmed that a large area of the perivascular tissue was ablated (>5 mm) in a single quadrant without significant damage to the renal artery. Our proposed device allows for control of the ablation position and produces deep nerve ablation without overheating the intima or surrounding blood, suggesting a highly capable new denervation catheter.

key words: *treatment-resistant hypertension, renal denervation (RDN), radio frequency (RF) current, microwave energy, coaxial-slot antenna.*

1. Introduction

The number of hypertensive patients in Japan is estimated to be about 43 million [1]. It is widely known that hypertensive patients have a significantly increased risk of life-threatening diseases such as myocardial infarction, stroke, and chronic kidney disease, as well as of all-cause mortality, with an estimated 100,000 deaths annually attributable to hypertension [1]. Thus, hypertension clearly has a negative impact on health, and hypertension treatment centered on antihypertensive drugs is being diligently implemented. On the other hand, about one-tenth of all hypertensive patients do not reach optimal blood pressure even after taking three or more antihypertensive medications, and additional treatment options are needed for these patients [1].

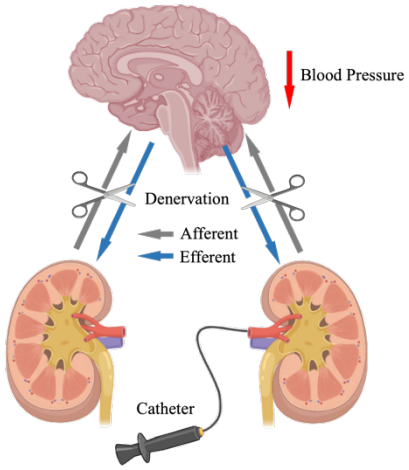

Fig. 1 Schematic of renal denervation (RDN). A catheter is inserted into the renal artery to ablate the renal sympathetic nerves around the vessel, thereby reducing blood pressure.

About a decade ago, a radio frequency ablation catheter has been introduced into the renal artery to ablate sympathetic nerve fibers around the renal artery from inside the vessel to suppress sympathetic nerve activity and achieve a hypotensive effect in patients with treatment-resistant hypertension; a new treatment method called “renal denervation (RDN)” [2] has been developed, and its clinical application is under investigation (Figure 1). The indication is not limited to patients with treatment-resistant hypertension, but is attracting considerable attention as a partial replacement for conventional drug therapy because it offers a new option for hypertension treatment using medical devices, where antihypertensive drugs were the only available treatment [3].

In recent years, various ablation catheters for RDN have been developed and tested in clinical trials. Although early small clinical trials showed promise for antihypertensive efficacy [4], subsequent large randomized controlled trials aimed at regulatory approval were not always favorable [5]. Despite this setback, several clinical trials have confirmed the efficacy and safety of RDN [6]-[9], and the current focus is on optimizing the treatment.

†The author is with Chiba University, Chiba-shi, 263-8522 Japan.
††The author is with The University of Tokyo Hospital, Bunkyo-ku, Tokyo, 113-8655 Japan.
†††The author is with The University of Tokyo, Bunkyo-ku, Tokyo, 113-8654 Japan.
††††The author is with the National Cancer Center, Kashiwa-shi 277-8577 Japan.

One possible reason for the failure of the clinical trial was thought to be an incomplete nerve ablation. This was attributed to the limited extent of ablation as well as to the lack of reproducibility of the technique [10]. Therefore, we opted to utilize microwave energy for RDN and explored a catheter design that enables consistent and standardized technique execution [11].

2. Microwave suitability for denervation

Several factors have been analyzed as contributing to the failure of large clinical trials of RDN, and one major factor is that the depth of ablation was shallow (2-4 mm) and the autonomic nerves may not have been sufficiently ablated and inactivated [12][13]. Many early ablation devices employed radio frequency (RF) current on the order of several hundred kHz as the energy source for nerve ablation [5], [14]-[17]. The RF catheter has an electrode at the tip, which is pressed against the intima of the blood vessel. The tissue in contact with the electrode is heated by joule heating, and the nerves located deep within are ablated by thermal conduction [18]. This is a direct adaptation of the more than 20-year-old technique of myocardial ablation for arrhythmias to nerve ablation. However, unlike arrhythmia treatment, in which it is sufficient to ablate the myocardium directly under the catheter, the nerve, which is the target tissue for denervation treatment, is also located deep in the vessel (> 5 mm) [19]. When attempting to ablate this area with RF contact heating, the thermal damage to the endothelium immediately below the catheter becomes too severe. In order to avoid this problem, lower input power is used, but leads to insufficient ablation. In addition, the perivascular tissues, lymph and tendons, redirect the RF current, and veins act as energy sinks [20]. As a result, it is thought that a clear antihypertensive effect may not be seen. Subsequent studies have shown that the distance from the vessel wall to the nerve is closer in the distal renal artery and renal artery branches, and that simultaneous treatment of the distal and branching arteries allows for better denervation [19][21].

We have been studying the medical application of the temperature increase that occurs when high-power microwaves are applied to biological tissue [22]. Microwave antennas can be fabricated into small diameters and are considered suitable for catheter applications. Furthermore, we considered that the heating principle is more suitable for denervation than RF current. Therefore, we plan to develop a new intravascular ablation catheter using microwaves. Figure 2 shows the difference between RF and microwave heating for myocardial ablation and endovascular denervation. Microwaves can heat tissue without contacting target because the energy can be transmitted away from the antenna. Heat in the tissue is spread by heat conduction, resulting in a temperature gradient [23]. In addition, the intima of the vessel is constantly cooled by the continuous blood flow to reduce thermal damage. On the other hand, deep nerves can be effectively ablated, as the cooling impact

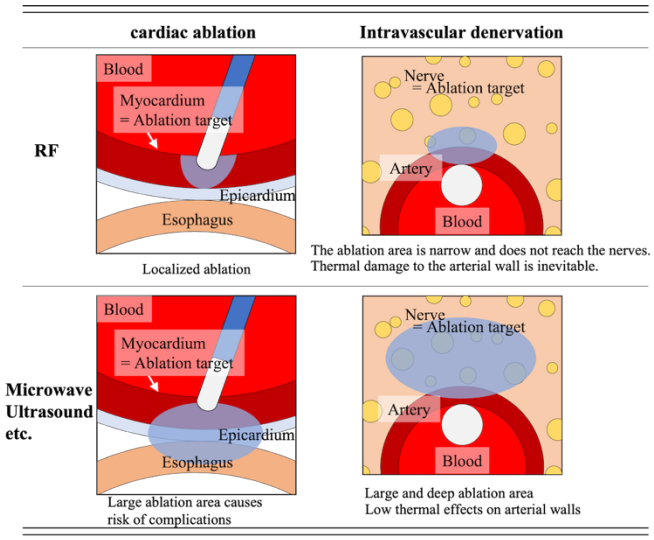

Fig. 2 Differences between cardiac ablation and intravascular denervation. RF, with its localized ablation area, is not suitable for denervation. Microwave, with their wide and gentle ablation areas, are not suitable for cardiac ablation but may be suitable for denervation.

of arterial blood flow is minimal. Our research has shown that microwaves can provide deeper heating with lower maximum temperatures than RF [18], but many issues remain for clinical use, such as heat generation in cables. Previously, a microwave denervation device was proposed in [24]. However, the design of this device places the antenna at the center of the vessel in a basket mechanism. Although this design allows for ablation of the entire circumference of the vessel in a single pass, it is thought that antenna misarranged from the center of the blood vessel can cause a bias ablation. Furthermore, the microwave output should be changed according to the blood vessel diameter.

The purpose of this study is to address the remaining issues with these microwave catheters and to develop a clinically relevant catheter. The antenna was optimized by computer simulation, and proof of concept was performed by *in vitro* and *in vivo* experiments.

3. Catheter design and numerical calculation

3.1 Design Overview

In our previous studies [18], the antenna was placed directly in the center of the simulated vessel, but in clinical practice, the antenna position must be reproducible. In addition, the coaxial-slot antenna used in that study can produce a circular ablation area while keeping the size and diameter small, but its dimensions have not been optimized for operation in the blood vessel. Therefore it is necessary to determine dimensions that can accommodate manufacturing variations and complex perivascular tissues.

In order to be applied to a catheter that can be used clinically, the following three conditions must be met: (1) the location of the ablation must be controllable (The ablation area per procedure should be approximately one quadrant of

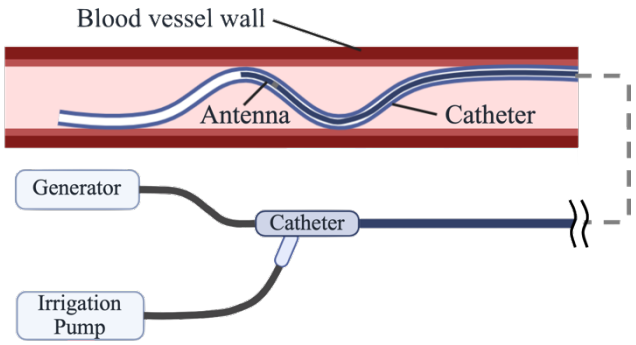

Fig. 3 Catheter structure and system overview. Microwaves generated by the generator are transmitted to the antenna inside the catheter. Perfusion fluid flows inside the catheter by an irrigation pump to cool the transmission cable.

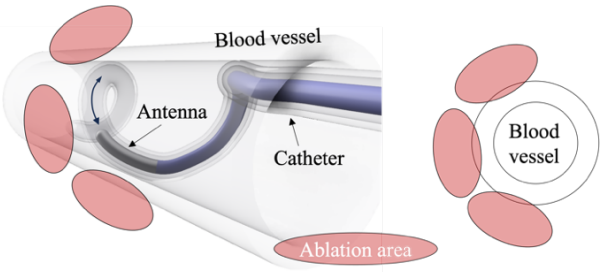

Fig. 4 A view of a spiral-shaped catheter operating in a blood vessel. The antenna can be moved within the catheter to control the direction of ablation.

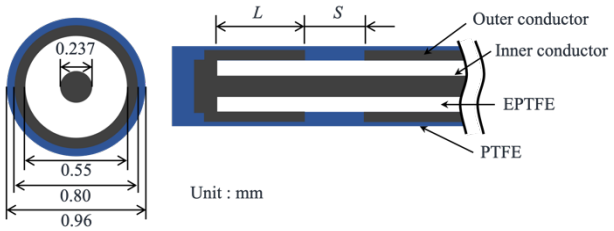

Fig. 5 Coaxial-slot antenna. The inner and outer conductors are copper. The insulation of the coaxial cable is expanded polytetrafluoroethylene (EPTFE) with a high air content. The coating is polytetrafluoroethylene (PTFE). Where L is the distance from the antenna tip to the slot and S is the width of the slot.

the vessel cross section), (2) deep nerve ablation must be possible (> 5 mm), and (3) the intima and surrounding blood flow must not be overheated (Endothelial loss must be < 50 % of vessel circumference and medial change depth must be < 50% of media thickness).

Figure 3 and Figure 4 show an overview of system and the proposed catheter structure. An open irrigation system is employed to cool the coaxial cable, and the lumen of the catheter is irrigated with cooling water (saline solution). The catheter tip is open and saline solution flows out into the blood vessel. The flow rate is about 30 ml/min, which is comparable to the perfusion volume used in cardiac ablation, and the health impact of the perfusate is considered small [25]. The irrigation system keeps the surface temperature of the catheter below 43 °C. The catheter is shaped into a helix, and the outer surface of the catheter contacts the vessel lumen. The helix diameter is about 4-8 mm, pitch is about 10-20 mm, and deforms to fit the vessel. The antenna is movable inside the catheter, and its movement in the helix determines the direction of ablation. The detailed procedure flow is as follows. The catheter is advanced into the renal artery along the guidewire. The guidewire and antenna are switched, and the antenna is advanced to the helix of the catheter. The position of the antenna is adjusted in the direction of the desired ablation, and microwaves are outputted from the generator. At the same time as the output, coolant is irrigated into the catheter from a pump.

The helix structure and cooling system allows (1) control of the ablation position and (2) deep nerve ablation because the irrigation system enables high power ablation due to cooling. The cooling effect of the irrigation system and blood flow suppresses (3) heating of the intima of the blood vessel and surrounding blood. The helix shape reduces the risk of vessel stenosis because the ablation is not all around the same section of the vessel. In addition, the catheter can be made smaller in diameter (6Fr : 2 mm), allowing a radial artery approach and minimally invasive procedures [26].

Figure 5 shows a coaxial-slot antenna, which is the antenna of this device [27]. In this antenna, the tip of the inner and outer conductors are shorted. This type of antenna can create a circular ablation area while keeping the diameter the same as a coaxial cable and has been used in our previous studies [28][29]. The design requirement for the reflection coefficient of the antenna should be less than -15 dB at 2.45 GHz (approximately 97% of the energy reaching the antenna is radiated). This requirement should also be followed even with slight dimensional variations. The radiated energy distribution should be concentric in the radial direction, and the ratio of axial to radial ablation area should be less than 2:1.

3.2 Catheter Design

The catheter design poses considerable technical challenges, primarily revolving around the requirements of shape memory and flexibility. Specifically, the catheter must exhibit a softer characteristic than the guidewire, allowing it to straighten out upon guidewire insertion, and subsequently revert to its original helix shape upon guidewire removal. Simultaneously, the catheter needs to possess greater stiffness compared to the antenna, ensuring it maintains its helix configuration during antenna insertion.

To address these challenges, catheters were manufactured utilizing thermoplastic elastomers with appropriate hardness. Figure 6 shows the catheter configuration during guidewire insertion, removal, and antenna insertion. Upon guidewire insertion, the helix straightened into a linear form; upon guidewire removal, the helix resumed its helix shape. The helix shape was maintained during antenna insertion, with the helix diameter changing from 6.8 to 7.9 mm and the pitch changing from 12.5 to 17.3 mm.

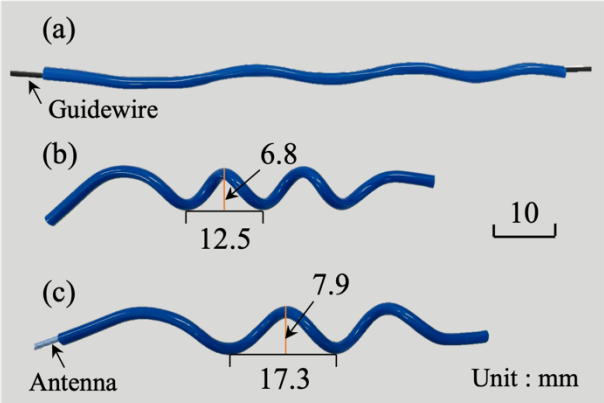

Fig. 6 Catheter shape when (a) guidewire is inserted, (b) guidewire is removed, and (c) antenna is inserted.

3.3 Numerical Calculation

Figure 7 shows the simulation model. The perivascular tissue used in this study was uniform fat tissue. A cylinder of blood and a vessel wall are placed concentrically in the center of the rectangular fat. The catheter is placed in contact with the vessel wall. Saline solution and a coaxial-slot antenna are placed concentrically in the catheter. The distance from the feeding point to the slot is 10 mm, so short that losses in the cable are almost negligible.

The simulations were performed with the finite integration solver of the electromagnetic simulator CST studio suite 2022 (Dassault systems, Vélizy-Villacoublay, France). Reflection coefficients of the antenna at frequencies from 1 to 4 GHz were calculated to adjust the antenna parameters. Boundary conditions used a perfectly matched layer (PML). As no significant discrepancies were observed in the calculated results using this domain size, it was considered along with these boundary conditions for this study. The minimum and maximum cell sizes of the simulation model were 0.03 mm and 0.452 mm. The operating frequency of the antenna was set to 2.45 GHz, one of the ISM (Industrial, Scientific and Medical) frequencies in Japan, and L (the distance from the antenna tip to the slot) and S (the slot width) were determined at which the antenna reflection coefficient was minimal at this frequency. The dielectric properties at 2.45 GHz for each material used in the simulations are listed in Table 1. The dielectric properties were taken from the database [30] for the biological tissue, from the coaxial cable specifications for EPTFE, from the CST material library for PTFE and copper, and from the values measured using a vector network analyzer (P9370A, Keysight Technologies, California, USA) and dielectric measurement probe (HP85070, Hewlett Packard, California, USA) for the egg white and the saline, respectively. Here, the frequencies at which dielectric constants were measured ranged from 1 to 5 GHz (10 MHz span) and were calibrated by air, short circuit, and deionized water at 17.2 ℃. The temperature of the egg whites was 19.1 ℃. (Simulation in egg white is described in Section 4)

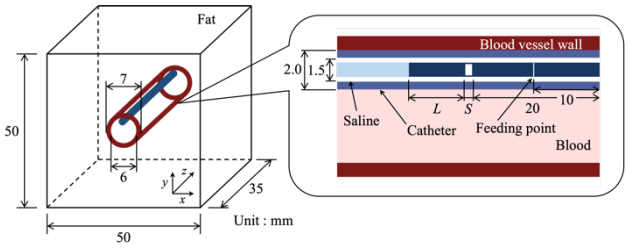

Fig. 7 Simulation model. A cylinder of blood and a vessel wall are placed concentrically in the center of a rectangular fat. The catheter is placed in contact with the vessel wall. Saline solution and a coaxial-slot antenna are placed concentrically in the catheter.

Table 1 Dielectric properties for each material used in the simulation @ 2.45GHz

Material	ε_r	σ [S/m]
Blood	58.3	2.54
Blood vessel wall	42.5	1.44
Fat	10.8	0.27
Muscle	52.7	1.74
Saline	77.1	2.93
Egg white	66.9	2.31
EPTFE (Dielectric for coaxial cable)	1.13	0.0
PTFE (Antenna coating, Catheter)	2.10	0.0
Copper (Outer, Inner conductor)	-	5.96×10^7

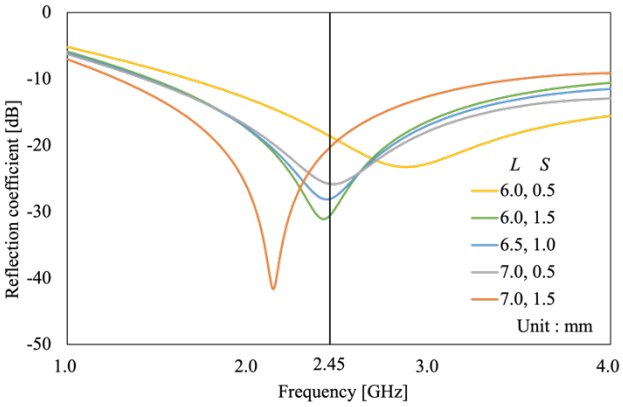

Fig. 8 Simulation results for each parameter (L, S). The horizontal axis is the frequency and the vertical axis is the reflection coefficient.

Figure 8 shows the simulation results of reflection coefficients when L and S are varied. The figure shows that the frequency at which the reflection coefficient reaches a minimum ($\boldsymbol{f_{res}}$) is close for antennas with the same $L + S$ (e.g. L = 6.0 mm, S =1.5 mm and L = 7.0 mm, S = 0.5 mm). When $L + S$ = 7.5 mm, the $\boldsymbol{f_{res}}$ is around 2.45 GHz. When

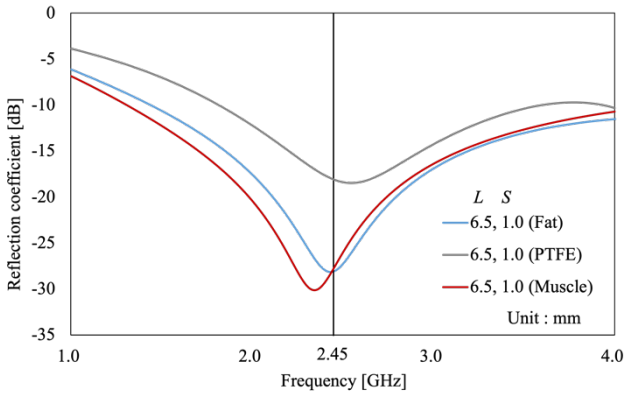

Fig. 9 Simulated antenna reflection coefficients when perivascular tissue is fat and when fat is replaced by PTFE and muscle (L = 6.5 mm, S = 1.0 mm).

S was fixed, f_{res} shifted toward lower frequencies as L increased, and when L was fixed, f_{res} also shifted toward lower frequencies as S increased. In both cases, this is thought to be due to the fact that the resonant frequency of the high-frequency current that can be distributed in this area has decreased due to the expansion of the L and S areas, which in effect act as antennas. At the operating frequency of 2.45 GHz, the lowest reflection coefficient was obtained at L = 6.0 mm and S = 1.5 mm with a value of -30.6 dB. The next lowest reflection coefficient was obtained at L = 6.5 mm, S = 1.0 mm, with a value of -28.1 dB. If we consider a coaxial-slot antenna as a kind of dipole antenna with a slot as a feeding point [27], the reflection coefficient of $L + S$ is considered to be minimal at about 1/4 wavelength in the medium. 2.45 GHz microwaves in blood (ε_r = 58.3) have a wavelength of 16.0 mm and it's 1/4 wavelength is 4 mm. As shown in Figure 5, the coaxial-slot antenna is not in direct contact with the blood, but has a PTFE (ε_r = 2.10) coating and catheter. The presence of a material with low relative permittivity in the surrounding area slightly lengthens the effective wavelength, and the point at which the reflection coefficient becomes minimal is probably larger than 4 mm.

All combinations of L = 6.0, 7.0 mm and S = 0.5, 1.5 mm had reflection coefficients below -15 dB at 2.45 GHz. It is suggested that adopting these central values makes it easier to cope with changes in antenna efficiency due to variations in manufacturing, differences in the vascular ambient environment, and changes in dielectric constant due to temperature changes. Therefore, the central values of L = 6.5 mm and S = 1.0 mm were used in this study.

The main assumptions made in this simulation are that the catheter is a straight line rather than a helix, that the perivascular tissue is uniform fat, and that the effect of temperature changes due to ablation on dielectric properties is not considered. Regardless of whether the catheter is straight or spiral, the simulation model assumes that the catheter is in contact with the vessel wall. Additionally, upon examining the local area surrounding the antenna, regardless of the perivascular tissue type and catheter shape, the components remain consistent: saline, catheter, blood, and vessel wall. Therefore, to simplify the model, the catheter was assumed to be straight and the perivascular tissue uniform. In the context of the temperature-dependent dielectric properties, the dielectric constant and conductivity decrease with decreasing water content when heated, particularly in high water content tissues [31]. According to [32], when liver is heated at 100 ℃ for 600 s, the dielectric constant decreases from 45.3 at 37 ℃ to about 25 and the conductivity decreases from 1.62 at 37 ℃ to about 1.1. In order to study the effect of complex perivascular tissues and change in dielectric properties due to temperature, we simulated the reflection coefficient of the antenna when the perivascular tissues were muscle and PTFE as an extreme case (Figure 9). Since muscle has a high dielectric constant and conductivity and PTFE, although not a tissue, has a very low dielectric constant and conductivity, it can be assumed that the values are between these two values in the dielectric properties of the complex perivascular tissue and in the dielectric properties that change with heating.

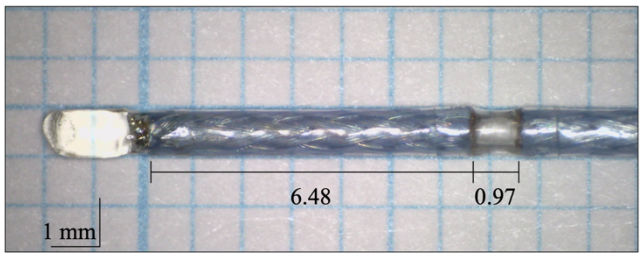

Fig. 10 Prototype coaxial-slot antenna. L : 6.48 mm, S : 0.97 mm

When the perivascular tissue is composed of PTFE, the resonant frequency is 2.55 GHz, shifted 0.10 GHz higher from 2.45 GHz. The reflection coefficient at 2.45 GHz was -18.1 dB. In the case of muscle tissue, the resonant frequency is 2.34 GHz, shifted 0.11 GHz lower. The reflection coefficient at 2.45 GHz was -27.7 dB. These values satisfy the antenna's requirement of less than -15 dB reflection coefficient, demonstrating that the antenna functions effectively over a wide range of relative permittivity (ranging from 52.7 to 2.1) and conductivity (ranging from 1.74 S/m to 0.0) of the perivascular tissues. This is due to the presence of saline, catheter, and blood directly below the antenna, which contribute more to the antenna's reflection coefficient than the perivascular tissues. Therefore, variations in dielectric properties caused by temperature rise or complex perivascular tissues are believed to have minimal impact on antenna matching.

4. *In vitro* experiment

4.1 Experimental Setup

Based on the simulation results, it was determined that an antenna with dimensions of L = 6.5 mm and S = 1.0 mm was optimal. Consequently, the antenna was fabricated with these specific dimensions in mind. A prototype of the proposed coaxial-slot antenna is shown in Figure 10. The

fabricated antenna was measured by a measuring microscope (MF-A1010D, Mitutoyo Corporation, Kanagawa, Japan) (L : 6.48 mm, S : 0.97 mm). The antenna was inserted into a catheter and the catheter lumen was filled with saline solution. The reflection coefficient of the fabricated antenna in egg white was measured by a vector network analyzer. The length of the feedline was approximately 70 cm. The cable loss was measured by a vector network analyzer and subtracted from the measured reflection coefficient. Here, the frequency range is 1 to 4 GHz (10 MHz span) and the IF bandwidth is 100 kHz.

The fabricated antennas were used for ablation experiments with egg whites. Experiments with egg white are often used to evaluate microwave ablation, and since the egg white denatures at about 60 ℃, the heating performance of the antenna can be visually evaluated [33]. A microwave generator (GMS200, Sairem, Décines-Charpieu, France) was used to generate a continuous wave signal at 2.45 GHz, which was transmitted to the antenna via coaxial cable. The power input to the antenna and the reflected wave were measured by a directional power sensor (NTR-Z44, Rohde & Schwarz , München, Germany). The generator output was adjusted to account for losses in the cable so that the radiated output from the antenna was 35 W. The antenna was placed in the catheter in the egg white, and the catheter was perfused with saline solution at a flow rate of 30 ml/min. The catheter lumen and the container of the egg white were completely separated, and the saline solution was released externally. The temperature of the egg white before microwave irradiation was 19.4 ℃ . All of the above temperatures were measured by a high-precision digital standard thermometer (ADS-100-HQ-150, Andokeiki Co., Ltd., Tokyo, Japan). Microwaves were irradiated to the egg whites for 180 seconds, photographs of the ablation area in the egg white were taken at 60, 120, and 180 seconds.

4.2 Results

Figure 11 shows the measured reflection coefficient in the white egg and simulation result when the same antenna and catheter were placed in egg white. There is a relatively good agreement between simulations and experimental reflection coefficient, i.e. ~300 MHz discrepancy in the resonant frequency and ~2 dB in the magnitude at the resonant frequency. The reflection coefficient of the fabricated antenna was -23.6 dB at 2.45 GHz. Figure 12 shows the simulated specific absorption rate (SAR) distribution in egg white (y-z plane), with contours at 20, 50 and 150 W/kg. The 150 W/kg contours were farthest from the catheter near the slot and closer to the catheter at the apical and basal ends of the slot. The 50 W/kg contours were gentle and elliptical in shape.

Figure 13 presents sequential snapshots of the egg white taken at 60 s intervals. Figure 14 also shows an extracted contour of the area where the egg white was denatured from the image. The egg white underwent thermal denaturation,

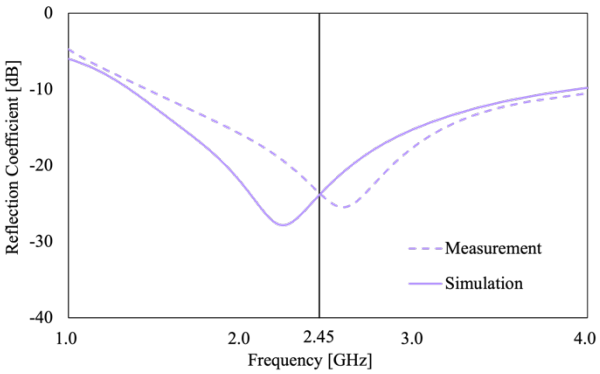

Fig. 11 Reflection coefficient of the antenna when the ambient environment is egg white. Solid orange lines are simulation results, dotted blue lines are measurement results.

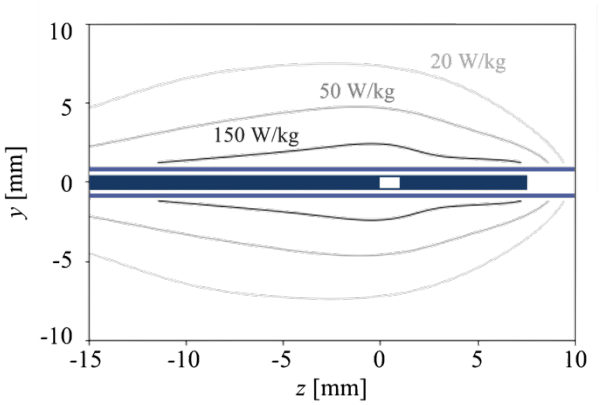

Fig. 12 SAR distribution when the ambient environment is egg white (simulation results). The input power is 1 W.

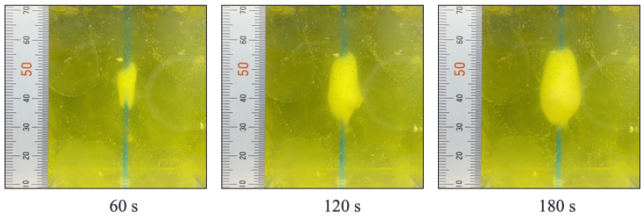

Fig. 13 Snapshot of egg whites during microwave irradiation (35 W). The protein in the egg white denatures and turns white as the temperature rises, and the area of discoloration expands with time.

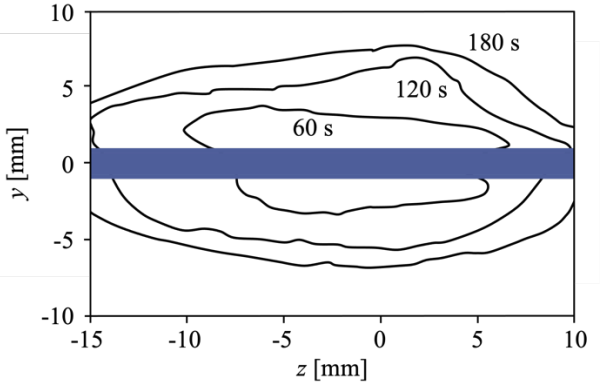

Fig. 14 Contour of the area where the egg white was denatured.

and the resulting ablated area is clearly visible. Denaturation initially occurred near the slot's position, with a subsequent expansion along the catheter axis resulting in denaturation covering an area of 26.5 mm at 180 s. In the radial direction, degeneration was observed as concentric circles at a distance of 6.2 mm from the catheter surface. At 60 s, the denatured region of the egg white at slightly more proximal than the slot is the largest, with little to no denatured region observed at the distal and proximal ends of the antenna. This pattern resembles the contours of the 150 W/kg SAR distribution simulated in Figure 12. It is known that the temperature distribution resulting from microwave irradiation over a relatively short period of time exhibits similarity to the SAR distribution [34], indicating that the denatured region of the egg white at 60 s closely aligns with the SAR distribution. Although simple comparisons cannot be made because thermal diffusion and convection are included in the results, the maximum radial distance of the 20 W/kg contour in Figure 12 is 6.3 mm, which is particularly similar to the contour of the denaturation region at 180s. The calculated values of the reflection coefficient closely matched the measured values of the prototype antenna. Moreover, the SAR distribution closely correspond to the discolored region of the egg white, indicating the validity of the electromagnetic field simulation.

CST also has the capability to perform thermal simulations using the results of electromagnetic field simulations, but it can only reproduce the effects of blood flow by assuming a constant temperature in the blood region. This assumption is equivalent to assuming that the blood flow velocity is infinite and overestimates the cooling effect. In addition, it is difficult to reproduce the tissue structure in the simulation because the perivascular tissue, which is the tissue to be heated in the actual living body, is complicated with nerves, fat, lymph, and so on. Therefore, it is necessary to confirm *in vivo* the heating by the antenna in the blood vessels.

5. *In vivo* experiment

5.1 Experimental Setup

In vivo experiment was performed on a male swine to see the area of RDN ablation and vascular damage caused by the proposed device and euthanized 2 weeks after treatment. The study protocol was approved (approval number IVT21-97) by the Animal Welfare Committee of the animal testing facility IVtech, Inc.

Under general anesthesia, a sheath was inserted percutaneously by standard technique, and heparin was administered intravenously at a dose of 200 U/kg. 0.035-inch guidewire was preceded into the artery under fluoroscopy, and a catheter was inserted into the renal artery. The catheter was checked to ensure that it was in contact with the vessel lumen, the antenna position was adjusted, and the catheter was ablated once for each artery. The reflection coefficient of the antenna were measured by a vector network analyzer. The length of the antenna feedline was approximately 70 cm, and the cable loss was measured with a vector network analyzer and subtracted from the reflection coefficient.

Before euthanasia, renal angiography was performed again under general anesthesia. At autopsy, the entire perirenal tissue and blood vessels were removed for histological evaluation at autopsy. The aorta was perfused with phosphate-buffered saline (PBS) with heparin (1000 U/L) from within the aorta, and then perfused with 10% neutral buffered formaldehyde (10% NBF). Tissues were then placed in containers and immersed in 5-10x volume of 10% NBF for about 1 week. After formalin fixation, hematoxylin and eosin (HE) staining and movat pentachrome (MP) staining were performed on the renal artery and perivascular tissue. The ablation area were identified by fibrosis, vacuolation, connective tissue coagulation, presence of hemorrhage or macrophages, etc. Safety criteria in animal studies include avoiding dissection of blood vessels, significant stenosis, impaired peripheral blood flow, or damage to other organs. Additionally, criteria involve preventing vascular endothelial loss or a decrease in media thickness that surpasses the impact observed with RF devices.

5.2 Results

The reflection coefficient of the antenna in one renal artery measured by a vector network analyzer is shown in Figure 15. The simulation results for the case L = 6.5 mm and S = 1.0 mm in Figure 8 are shown in the same figure. The frequency at which the reflection coefficient was minimum was 2.50 GHz in the renal artery, which was close to 2.45 GHz. The results are in good agreement with simulations, with a reflection coefficient of -32.0 dB at 2.45 GHz.

Angiographic images of the renal artery are shown in Figure 16. The diameter of the renal artery was 5.9 mm. The diameter of the renal artery was determined on the image using the diameter of the catheter (2 mm) as a reference. Initially, the catheter was straightened using a guidewire and

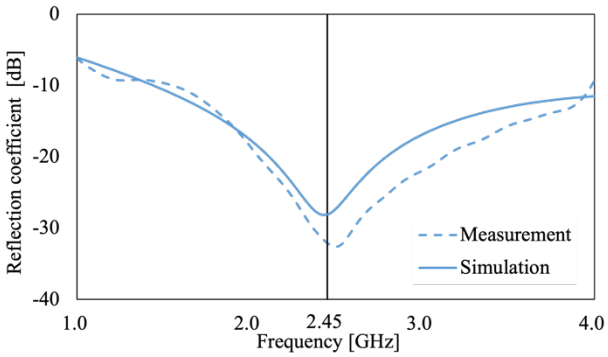

Fig. 15 Reflection coefficient of the antenna within the renal artery. Solid orange lines are simulation results, dotted blue lines are measurement results.

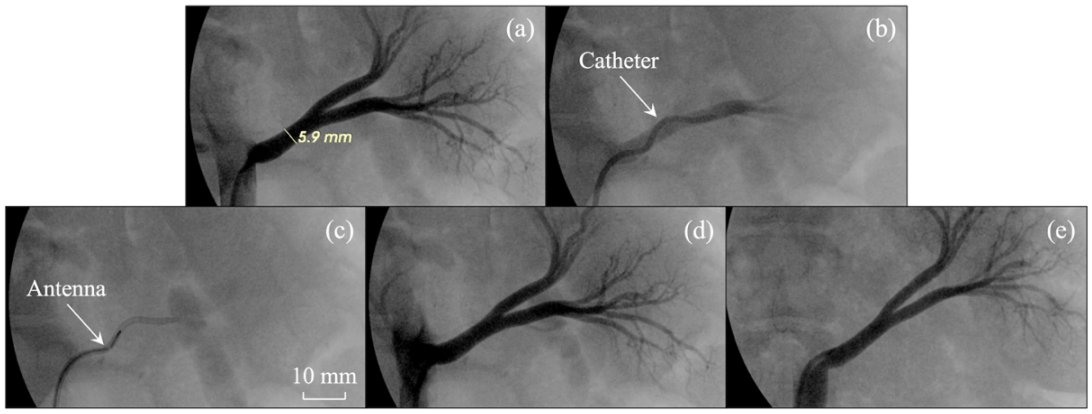

Fig. 16 Microwave catheter deployment and angiography. (a) Renal arteriography before ablation. (b) Deployment of the catheter, the outer surface of the spiral catheter contacting the vessel lumen. (c) Insertion of the antenna to the desired ablation position. (d) Angiography immediately after ablation. (e) Angiography 2 weeks after the procedure.

successfully navigated to the renal artery without complications. Upon removal of the guidewire, the catheter resumed its helix shape and was confirmed, via angiography, to be in direct contact with the vessel wall. Even after the antenna was inserted, the catheter maintained its helix shape within the renal artery, consistently in contact with the vessel wall. The slot, the center of the ablation, was placed caudally and the ablation was performed at 50 W for 60 s. (The generator output was adjusted to account for the cable loss so that the energy radiated from the antenna was 50 W.) Both angiography images, immediately after ablation and 2 weeks later, showed no problems with the vessels immediately above the ablation or the blood flow in the periphery. Figure 17 shows a pathology image (HE stain) of the ablated renal artery and perivascular tissue. The image with the largest ablation area was identified in the acquired image. The ablated area of the perivascular tissue is shown. The image confirmed that the ablation direction focused toward the left side of the image, it can be seen that the ablation direction is controlled. In addition, the maximum depth of tissue denatured by heat is 14.4 mm, confirming that the thermal effect extends deep into the perivascular tissue. There is also thermal influence on the vessel wall in the left down direction, but endothelial loss is less than 25% of the circumference of the vessel, and the media thickness changes at a rate of less than 25%. This is grade 1 on the standardized vascular injury score [35] (The higher the number, the more severe the damage). In RF devices reported [36], medial depth change was grade 4 and damage was severe, suggesting microwave superiority. Although the lymph node is included in the ablation area, nonclinical studies of existing products have also confirmed ablation of lymph nodes [20][21], and this is not considered a major safety concern.

6. Discussion

We proposed a new microwave catheter for RDN. The antenna design utilized a coaxial slot antenna, and its dimensions were optimized by calculating the reflection coefficient through simulations. The reflection coefficient is the most important parameter determining the radiation efficiency of the antenna. The simulations do not replicate the blood flow and the complexity of surrounding organs, thus thermal predictions are not included. Based on the simulation results, the dimensions were optimized to L = 6.5 mm and S = 1.0 mm. The measured reflection coefficient of the fabricated antenna closely matched the calculated values, achieving a reflection coefficient of -32.0 dB @ 2.45 GHz in *in vivo* measurements. The design of this antenna allows for accommodating manufacturing tolerances, complex biological structures, and variations in dielectric properties due to temperature changes. Compared to our existing antennas [18], by using the antenna that can maintain constant radiation efficiency regardless of the environment, the stability of the procedure can be improved and consistent treatment results can be obtained.

This catheter features a helix shape and an irrigation system, enabling control of the ablation direction, high-power heating, and reproducible technique. The helix shape ensures that the observed ablation region on the vessel cross-section is not fully circumferential, while the irrigation system cools the vessel lumen, reducing the risk of vascular stenosis. Animal experiments have shown lower vascular damage compared to RF devices reported in [36]. Despite the small vascular damage, the ablation extends up to a depth of 14.4 mm from the vessel lumen, which is sufficient for ablating the surrounding nerves. *In vitro* experiments with egg whites show cauterization over the entire circumference of the catheter, whereas *in vivo*, the helical shape of the catheter keeps it in contact with the lumen of the vessel, and the thermal effect on the opposite tissue is minimal. The ablation area is approximately confined to a single quadrant, and complete ablation of the entire circumference of the blood vessel is achieved by performing multiple ablations along the helix.

Technologies other than RF, such as ultrasound and alcohol injection, have been proposed for RDN, aiming for deeper ablation methods to achieve effective denervation [37][38]. Alcohol injection requires inserting a needle from

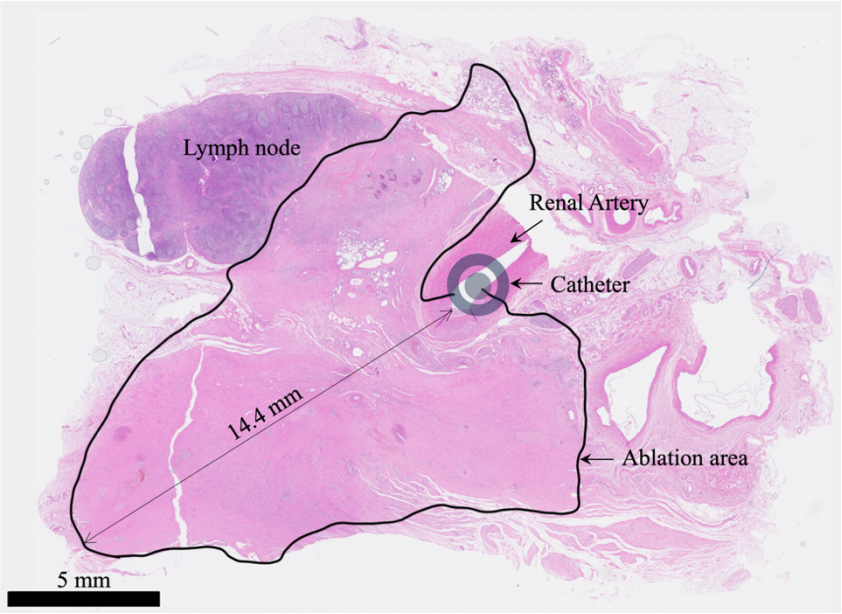

Fig. 17 Pathological image of renal artery and perivascular tissue. The vessel in the center is the renal artery (RA), and the ablated area is surrounded by black lines. Part of the lymph node is included in the ablation area.

the inside to the outside of the vessel, which poses a risk of vessel rupture when attempting to withdraw the catheter before removing the needle. Ultrasound devices, on the other hand, are thick and challenging to handle, and their non-compliant balloon design makes it difficult to accommodate different vessel diameters. The helix shape, with its ability to adjust the diameter to match the vessel size, offers potential for accommodating various vessel diameters compared to non-compliant balloons.

A drawback of microwave heating is the relatively longer heating time required. Representative RF devices like Symplicity Spyral perform ablation in four quadrants simultaneously in 60 s [39], and the ultrasound device Paradice recently achieved single ablation in 7 s [8]. For our proposed device, we estimate a time of 60-120 s for a single ablation, and multiple ablations are necessary for full circumferential ablation. However, the ablation time is not significantly longer compared to the overall procedure time.

The current *in vivo* experiments lack the gold standard measurement of renal norepinephrine concentration, a crucial metric for evaluating effectiveness [35]. Although a single ablation was performed on the renal artery in this study, determining the optimal output and number of ablation cycles required for completion should be guided by norepinephrine concentration and evaluating safety. Furthermore, future studies should focus on increasing the sample size and demonstrating both safety and efficacy for potential clinical application.

7. Summary

In this paper, we proposed a novel microwave catheter for RDN for treatment-resistant hypertension. The main features of the catheter are a thin coaxial slot antenna and a helix structured outer sheath. The dimensions of the antenna were determined by simulation. The measured reflection coefficient in the renal artery was -32 dB, which was sufficient for the antenna. The helix structure of the catheter allows for single quadrant ablation and stable technique independent of vessel diameter. *In vivo* experiments showed less vessel damage than RF, with successful ablation of up to 14.4 mm. In summary, our proposed microwave denervation catheter shows both safety and deep ablation, offering the potential to replace existing RDN devices.

Acknowledgments

A part of this study is supported by The Uehara Memorial Foundation.

References

[1] The Japanese Society of Hypertension., “Guidelines for the management of hypertension 2019,” Life Science Publishing, 2019.
[2] M.P. Scjlaich, P.A. Sobotka, H. Krum, R. Whitbourn, A. Walton, and M.D. Esler, “Renal denervation as a therapeutic approach for hypertension : novel implications for an old concept” Hypertension, vol.54, no.6, pp.1195-1201, 2009.
[3] R.E. Schmieder, K. Högerl, S. Jung, P. Bramlage, R. Veelken, and C. Ott, “Patient preference for therapies in hypertension: a cross-sectional survey of German patients” Clin. Res. Cardiol., vol.108, pp.1331-1342, 2019.
[4] F. Mahfoud, M. Schlaich, I. Kindermann, et al., “Effect of renal sympathetic denervation on glucose metabolism in patients with resistant hypertension : A pilot study,” Circ. J., vol.123, no.18, pp.1940-1946, 2011.
[5] G.L. Bakris, R.R. Townsend, M. Liu, et al., “Impact of renal denervation on 24-hour ambulatory blood pressure: results from SYMPLICITY HTN-3,” J. Am. Coll. Cardiol., vol.64, no.11, pp.1071-1078, 2014.

[6] F. Mahfoud, M, Böhm, R. Schmieder, et al., “Effects of renal denervation on kidney function and long-term outcomes: 3-year follow-up from the Global SYMPLICITY Registry,” Eur. Heart J., vol.40, no.42, pp.3474-3482, 2019.

[7] R.R. Townsend, F. Mahfound, D.E. Kandzari, et al., “Catheter-based renal denervation in patients with uncontrolled hypertension in the absence of antihypertensive medications (SPYRAL HTN-OFF MED): a randomised, sham-controlled, proof-of-concept trial,” Lancet, vol.390, no.10108, pp.2160-2170, 2017.

[8] M. Azizi, R.E. Schmieder, F. Mahfoud, et al., “Endovascular ultrasound renal denervation to treat hypertension (RADIANCE-HTN SOLO): a multicentre, international, single-blind, randomised, sham-controlled trial,” Lancet, vol.391, no.10137, pp.2335-2345, 2018.

[9] D.E. Kandzari, M, Böhm, F. Mahfoud, et al., “Effect of renal denervation on blood pressure in the presence of antihypertensive drugs: 6-month efficacy and safety results from the SPYRAL HTN-ON MED proof-of-concept randomised trial,” Lancet, vol.391, no.10137, pp.2346-2355, 2018.

[10] R. Glati, C.E. Raphael, M. Negoita, S.J. Pocock, and B.J. Gersh, “The rise, fall, and possible resurrection of renal denervation,” Nat. Rev. Cardiol., vol.13, pp.238-244, 2016.

[11] Kazuyuki Saito, "Development of microwave catheter for hypertension treatment," Research Report of The Uehara Memorial Fundation, vol. 36, Dec. 2022. (in Japanese)

[12] E.E. Vink, R. Goldschmeding, A. Vink, C. Weggemans, R.L.A.W. Bleijs, and P.J. Blankestijn, “Limited destruction of renal nerves after catheter- based renal denervation: results of a human case study,” Nephrol. Dial. Transplant., vol.29, no.8, pp.1608-1610, 2014.

[13] F. Mahfoud, E.R. Edelman, and M. Böhm, “Catheter-based renal denervation is no simple matter: Lessons to be learned from our anatomy?,” J. Am. Coll. Cardiol., vol.64, no.7, pp.644-646, 2014.

[14] D.L. Kandzari, K. Kario, F. Mahfoud, et al., “ The SPYRAL HTN global clinical trial program: Rationale and design for studies of renal denervation in the absence (SPYRAL HTN OFF-MED) and presence (SPYRAL HTN ON- MED) of antihypertensive medications,” Am. Heart J., vol.171, no.1, pp.82-91, 2016.

[15] S.G. Worthley, C.P. Tsioufis, M.I. Worthley, et al., “Safety and efficacy of a multi-electrode renal sympathetic denervation system in resistant hypertension: the EnligHTN I trial,” Eur. Heart J., vol.34, no.28, pp.2132-2140, 2013.

[16] G.J. Wilson, D. Winsor-Hines, R.R. Tunstall, et al., “Bipolar multi-electrode balloon catheter radiofrequency renal denervation with the Vessix system: preclinical safety evaluation,” EuroIntervention, vol.10, no.10, pp.1239-1246, 2015.

[17] J.A. Ormiston, T. Watson, N.V. Pelt, et al., “Renal denervation for resistant hypertension using an irrigated radiofrequency balloon: 12-month results from the Renal Hypertension Ablation System (RHAS) trial,” EuroIntervention, vol.9, no.1, pp.70-74, 2013.

[18] A. Rakhmadi, K. Saito, S. Matsuhara, T. Tajima, and N. Takeshita, ”Comparison of radio frequency current and microwave energy for transcatheter renal denervation,” IEEE J. Electromagn. RF Microw. Med. Biol., vol.4, no.2, pp.89-96, 2020.

[19] K. Sakakura, E. Ladich, Q. Cheng, et al, “Anatomic assessment of sympathetic peri-arterial renal nerves in man,” J. Am. Coll. Cardiol., vol.64, no.7, pp.635-643, 2014.

[20] A.R. Tzafriri, J.H. Keating, P.M. Markham, et al., “Arterial microanatomy determines the success of energy-based renal denervation in controlling hypertension,” Hypertension, vol.7, no.285, 2015.

[21] F. Mahfoud, S. Tunev, S. Ewen, et al., “Impact of lesion placement on efficacy and safety of catheter-based radiofrequency renal denervation,” J. Am. Coll. Cardiol., vol.66, no.16, pp.1766-1775, 2015.

[22] K. Saito, H. Yoshimura, K. Ito, Y. Aoyagi, and H. Horita, “Clinical trials of interstitial microwave hyperthermia by use of coaxial-slot antenna with two slots,” IEEE Trans Microw Theory Tech, vol.52, no.8, pp.1987-1991, 2004.

[23] W. Schramm, D. Yang, B.J. Wood, F. Rattay, and D. Haemmerich, “Contribution of direct heating, thermal conduction and perfusion during radiofrequency and microwave ablation,” Open Biomed. Eng., vol.1, pp.47-52, 2007.

[24] P.C. Qian, M.A. Barry, J. Lu, et al., “Transcatheter microwave ablation can deliver deep and circumferential perivascular nerve injury without significant arterial injury to provide effective renal denervation,” Hypertension, vol.37, no.10, pp.2083-2092, 2019.

[25] M. H. Kanj, O. Wazni, T. Fahmy, et al., “Pulmonary Vein Antral Isolation Using an Open Irrigation Ablation Catheter for the Treatment of Atrial Fibrillation A Randomized Pilot Study,” J. Am. Coll. Cardiol., vol.49, no.15, pp.1634-1641, 2007.

[26] S. Saito, H. Ikei, G. Hosokawa, and S. Tanaka, “Influence of the ratio between radial artery inner diameter and sheath outer diameter on radial artery flow after transradial coronary intervention,” Catheter. Cardiovasc. Interv., vol.46, no.2, pp.173-178, 1999.

[27] K. Ito, and K. Furuya, “Basics of microwave interstitial hyperthermia,” Jpn. J. Hyperthermic Oncol., vol.12, no.1, pp.8-21, 1996.

[28] K. Saito, A. Hiroe, S. Kikuchi, M. Takahashi, and K. Ito, “Estimation of heating performances of a coaxial-slot antenna with endoscope for treatment of bile duct carcinoma,” IEEE Trans. Microw. Theory. Tech., vol.54, no.8, pp.3443-3449, 2006.

[29] K. Saito, Y. Hayashi, H. Yoshimura, and K. Ito, “Heating characteristics of array applicator composed of two coaxial-slot antennas for microwave coagulation therapy,” IEEE Trans. Microw. Theory. Tech., vol.48, no.11, pp.1800-1806, 2000.

[30] IT’IS Foundation., “Tissue properties database V4-1,” IT’IS Foundation, 2022.

[31] Y. Endo, Y. Tezuka, K. Saito, and K. Ito, “Dielectric properties and water contents of coagulated biological tissue by microwave heating,” IEICE Commun. Expr., vol.4, no.4, pp.105-110, 2015.

[32] C. L. Brace, “Temperature-dependent dielectric properties of liver tissue measured during thermal ablation: Toward an improved numerical model,” Annu. Int. Conf. IEEE Eng. Med. Biol. Soc., pp.230-233, 2008.

[33] Y. Mohtashami, S.C. Hagness, and N. Behdad, “A hybrid slot/monopole antenna with directional heating patterns for microwave ablation,” IEEE Trans. Antennas Propag., vol.65, no.8, pp.3889-3895, 2017.

[34] Y. Okano, K. Ito, I. Ida, and M. Takahashi, “The SAR evaluation method by a combination of thermographic experiments and biological tissue-equivalent phantoms,” IEEE Trans. Microw. Theory. Tech., vol.48, no.11, pp.2094-2103, 2000.

[35] K. Sakakura, E. Ladich, E.R. Edelman, et al., “Methodological standardization for the pre-clinical evaluation of renal sympathetic denervation,” JACC Cardiovasc. Interv., vol.7, no.10, pp.1184-1193, 2014.

[36] A. Sakaoka, H. Terao, S. Nakamura, et al., “Accurate depth of radiofrequency-induced lesions in renal sympathetic denervation based on a fine histological sectioning approach in a porcine model,” Circ. Cardiovasc. Interv., vol.11, no.2, 2018.

[37] T. Mabin, M. Sapoval, V. Cabane, J. Stemmett, and M. Iyer, “First experience with endovascular ultrasound renal denervation for the treatment of resistant hypertension,” EuroIntervention, vol.8, no.1 pp.57-61, 2012.

[38] T.A. Fischell, A. Ebner, S. Gallo, et al., “Transcatheter alcohol-mediated perivascular renal denervation with the peregrine system first-in-human experience,” JACC Cardiovasc. Interv., vol.9, no.6, pp.589- 598, 2016.

[39] D.E. Kandzari, K. Kario, F. Mahfoud, et al., “The SPYRAL HTN global clinical trial program: Rationale and design for studies of renal denervation in the absence (SPYRAL HTN OFF-MED) and presence (SPYRAL HTN ON- MED) of antihypertensive medications,” Am. Heart J., vol.171, no.1, pp.82-91, 2016.

Shohei Matsuhara was born in Hokkaido, Japan, in Nov 1994. He received the B.E., and M.E. degrees in medical engineering from Chiba University, Chiba, Japan, in 2017, 2019, respectively. He is currently working toward the Ph.D. degree at the Graduate School of Engineering, Department of Medical Engineering, Chiba University, Chiba, Japan.

His primary research interest is in the area of medical applications of electromagnetic field such as the development of microwave ablation catheters.

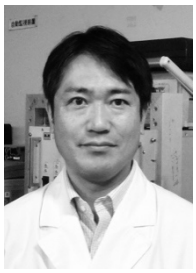

Kazuyuki Saito was born in Nagano, Japan, in May 1973. He received the B.E., M.E., and D.E. degrees in electronic engineering from Chiba University, Chiba, Japan, in 1996, 1998 and 2001, respectively. He is currently an Associate Professor with the Center for Frontier Medical Engineering, Chiba University. His main interest is in the area of medical applications of electromagnetic field including thermal treatment of cancer and microwave surgical devices etc.

Dr. Saito is a member of the Institute of Electrical and Electronics Engineers (IEEE), Institute of the Image Information and Television Engineers of Japan (ITE), the Japanese Society for Thermal Medicine (JSTM), and the Japan Society for Endoscopic Surgery (JSES). He received the IEICE AP-S Freshman Award, the Award for Young Scientist of URSI General Assembly, the IEEE AP-S Japan Chapter Young Engineer Award, the Young Researchers Award of IEICE, and the International Symposium on Antennas and Propagation (ISAP) Paper Award in 1997, 1999, 2000, 2004, and 2005 respectively.

Tomoyuki Tajima was born in Tokyo, Japan, in Nov 1981. He received an M.D. and Ph.D. degree from The University of Tokyo, Tokyo, Japan. He previously worked as a cardiologist at Japanese hospitals. His research focused on the genetic relationship between accumulations of rare variants and susceptibility of ischemic heart disease.

He joined the Japan-Stanford Biodesign fellowship, and then he founded a medical device startup Alivas, Inc. in which he is currently working as the CEO.

Aditya Rakhmadi was born in Jakarta, Indonesia, in 1994. He received the B.E. degree in electrical engineering from the University of Indonesia, West Java, Indonesia, in 2016, the M.E. and Ph.D. degrees in medical engineering from Chiba University, Chiba, Japan in 2020 and 2023, respectively. He is a member of the Institute of Electrical and Electronics Engineers (IEEE).

His research interests include antennas for communication, wearable antennas for medical applications, microwave energy devices for medical applications, and phantom development for evaluating electromagnetic effects. He received the IEICE Communication Express Top Downloaded Letter Award in 2020.

Yoshiki Watanabe was born in Kanagawa, Japan, in July 1994. He received the B.E. degree in medical engineering from Chiba University, Chiba, Japan, in 2017, and the M.E. degree in bioengineering from the University of Tokyo, Tokyo, Japan, in 2019. He is currently working toward the Ph.D. degree at the Graduate School of Engineering, Department of Bioengineering, the University of Tokyo, Tokyo, Japan.

His research interests include medical applications of electromagnetic field, ultrasound imaging, and physics-informed machine learning.

Nobuyoshi Takeshita received Ph.D. degree in medicine from Chiba University, Chiba, Japan. He is currently a surgeon in the Department of Colorectal Surgery/NEXT medical device innovation center at National Cancer Center Hospital East in Japan.

His research interest focused on minimally invasive treatment for the GI tract such as laparoscopic/robotic surgery and flexible endoscopy. To fill the gap between clinicians and engineers, he has generated many collaborations with med-tech start-ups, academics and clinicians in Japan and Singapore including surgical robots, neuro-modulators, tissue engineering, cancer diagnostic tools and AI-assisted systems/VR simulators for minimally invasive surgery.